J. Fluid Mech. (1991), *vol.* 229, *pp.* 29–50
Printed in Great Britain

Parametric resonance of a spherical bubble

By CHIANG C. MEI[1] AND XIANCHU ZHOU[2]
[1] Civil Engineering Department, Massachusetts Institute of Technology, Cambridge, MA 02139, USA
[2] Institute of Mechanics, Academia Sinica, Beijing, China

(Received 12 June 1990)

We modify a recent theory of Longuet-Higgins (1989*a*, *b*) to study the resonant interaction between an isotropic mode and one or two distortional modes of an oscillating bubble in water when the isotropic mode is forced by ambient sound. Gravity and buoyant rise are ignored. The energy exchange between modes is strong enough so that both (or all three) can attain comparable amplitudes after a long time. We show that for two-mode interactions the mode-coupling equations are similar to those studied in other physical contexts such as nonlinear optics, coupled oscillators and standing waves in a basin. Instability around fixed points is examined for various bubble radii, phase mismatch, and detuning of the external forcing. Numerical evidences of chaotic bubble oscillations and sound radiation are discussed. It is found that in a certain parameter domain, Hopf bifurcations are possible, and chaos is reached via a period-doubling sequence. However, when there are three interacting modes, each of the two distortion modes interacts with the breathing mode directly and the route to chaos is via a quasi-periodic 2-torus. Possible relevance of this theory to the observed erratic drifting of a bubble is discussed.

1. Introduction

A well-known phenomenon in bubble dynamics is the erratic drift of a bubble in an ambient sound field when the latter exceeds a certain threshold (Strasberg & Benjamin 1958). This phenomenon has been attributed to the subharmonic resonance of a shape-distortion mode with the isotropic breathing mode. A linearized theory of such resonance based on the Mathieu equation was proposed by Benjamin & Strasberg (1958) and Eller & Crum (1970). Subsequently Hall & Seminara (1980) gave a nonlinear theory by allowing the amplitude of a distortion mode to be $O(\epsilon) \ll 1$ ($O(\epsilon^{\frac{1}{2}})$ in their notation), and the breathing mode to be $O(\epsilon^2)$. Neglecting all damping mechanisms, they deduced a cubic evolution equation for the complex amplitude of the distortion mode, valid over the timescale $O(\epsilon^2\omega t) = 1$, where ω denotes the frequency. The breathing mode only acts as the background excitation and does not take part in the nonlinear evolution. Bifurcations as functions of the detuning frequency were examined. Since the complex equation corresponds to a first-order dynamical system with just two real degrees of freedom, no chaos was found.

Recently Benjamin & Ellis (1990) derived a formula for the drift velocity of an oscillating bubble as the consequence of second-order interactions between two neighbouring distortion modes. They also described new experiments showing the erratic drift. Since chaos is known to occur in the subharmonic resonance of standing surface waves in a basin (Gollub & Meyer 1983; Ciliberto & Gollub 1985; Feng &

Sethna 1989; Meron & Procaccia 1986; Simonelli & Gollub 1989; Kambe & Umeki 1990), they concluded by analogy that two neighbouring distortion modes of a bubble may also be chaotic, resulting in erratic drifting. A direct theory for the chaotic bubble oscillation to substantiate this conclusion is therefore desirable. Since at high modal numbers, two neighbouring distortion modes have nearly the same frequencies, they can be simultaneously resonated by ambient sound through the breathing mode. In principle it appears possible to extend the theory of Hall & Seminara (who focused their attention to the lowest mode with $n = 2$) to two distortion modes n and $n+1$ with large n, and derive a dynamical system with four degrees of freedom. Chaotic responses similar to those examined theoretically by Meron & Procaccia (1986), Feng & Sethna (1989) and Kambe & Ukema (1990) are highly likely. This mechanism, if proven, would then be a powerful one, since the breathing mode could be an order of magnitude smaller. On the other hand the growth rate would be rather low and the band of frequency mismatch must be very small ($\sigma_n - \sigma_{n+1} = O(\epsilon^2\omega)$).

As in standing waves in a basin (Kambe & Umeki 1990), there can be several mechanisms for parametric bubble resonance. Motivated by acoustic sensing of breaking waves on the ocean surface, Longuet-Higgins (1989*a*) has examined the opposite problem, i.e. how shape oscillations of a bubble with natural frequency σ_n can excite the breathing mode which radiates sound at $2\sigma_n$. This is a second-order theory of second-harmonic generation by quadratic coupling. Longuet-Higgins (1989*b*) also gives the transient solution for given initial shape distortion and calculates the damped oscillation of the second-order breathing mode, and the radiated sound. Various damping mechanisms have been included: acoustic, thermal and viscous, so that the amplitude of the breathing mode is finite even if the resonance condition, $\omega = 2\sigma_n$, is satisfied exactly, where σ_n is the natural frequency of the nth distortion mode. At resonance, the amplitude is inversely proportional to the total damping. Let the dimensionless damping coefficient be denoted by β/ω so that the amplitude decays as $\exp(-\beta t)$ in the linear theory. It is known (e.g. Prosperetti 1977) that the range of the combined damping coefficient is $\beta = 10^5$ to $10(1/\mathrm{s})$ for a bubble with radius ranging from 0.01 cm to 1 cm. The range of frequency of common interest in ocean acoustics is very broad: $O(100\ \mathrm{Hz})$ to $O(100\ \mathrm{kHz})$. Thus for sufficiently high frequency and large bubbles, damping can be very low. When persistent forcing is present the isotropic mode can be resonantly amplified to the extent that a second-order theory may no longer be sufficient. A nonlinear theory allowing both interacting modes to be of first order is therefore needed, and it would lead to another mechanism of parametric resonance.

Transient problems of quadratically coupled oscillators have been studied before in other contexts. A celebrated example is in optics (Armstrong *et al.* 1962), where for general initial conditions and negligible damping, energy can be interchanged periodically between the first and second harmonics (ω and 2ω). Later studies of forced resonance of quadratically coupled oscillators with linear frequencies ω_1 and ω_2 include the works of Sethna (1965) who analysed the equilibrium states (fixed points) and their stability. Hatwal, Mallik & Ghosh (1983) found numerically and experimentally signs of chaotic motion and suggested statistical representation of the results. Miles (1984) carried out a more systematic search for chaos. While the frequency ω_f of external forcing can be close to either $\omega_1 = 2\omega_2$ or ω_2, Miles focused his attention on forcing near the lower ω_2 only. For a special set of parameters which corresponds to exact phase matching, i.e. $\omega_1 = 2\omega_2$, he did not find a chaotic response for $\omega_f \sim \omega_1$. However, for a mathematically similar problem of standing gravity waves in a basin, Gu & Sethna (1987) have shown that Hopf bifurcations and chaos can occur if slight phase mismatch is allowed, i.e. $\omega_1 \approx 2\omega_2$.

With a view to finding chaotic subharmonic resonance we modify the work of Longuet-Higgins by including external forcing and by allowing the resonant responses of both interacting modes to be eventually comparable (i.e. both are of first order, in the normalized sense to be explained). Assuming that gravity is negligible so that the effects of buoyant rise are unimportant, we first show that the long-time evolution equations for the complex amplitudes of the two modes are of the same type as those studied by Armstrong *et al.*, Sethna and Miles. But for a bubble it is the forcing at the subharmonic frequency that is of physical interest here. Moreover, for an increasingly large bubble the natural frequencies of the distortion modes can be close, so that parametric resonance may involve more than two modes. Some consequences of three-mode interactions are studied here also. Since in nature, physical parameters such as the bubble radius may not correspond exactly to perfect phase matching: $\omega = 2\sigma_n$, chaos may therefore arise and is examined here.

Chaotic oscillations of bubbles were first shown in the pioneering works of Lauterborn and colleagues who studied isotropic modes of a spherical bubble with finite oscillation amplitude (see Lauterborn & Partilz 1988 for a review). The present work suggests that simple harmonic forcing can also excite chaotic oscillations of the isotropic mode through its interaction with one or more shape modes, and therefore can also lead to radiation of random signals to the far field. Combined with the theory of Benjamin & Ellis (1990), it also provides a possible basis for erratic dancing of bubbles in sound.

2. Order estimates

For reference we cite the well-known resonant frequency of an air-filled bubble of radius R without surface tension,

$$\omega_0 = \left(\frac{3\gamma P_b}{\rho R^2}\right)^{\frac{1}{2}} \tag{2.1}$$

(Minnaert 1933), where P_b is the air pressure in the bubble, γ is the ratio of specific heats of air, and ρ is the water density. Thus the ratio of bubble radius to sound wavelength/2π is

$$kR = \frac{\omega_0 R}{C} = \frac{1}{C}\left(\frac{3\gamma P_b}{\rho}\right)^{\frac{1}{2}}. \tag{2.2}$$

Taking $C = 150000$ cm/s, $\gamma = 1.4$, $\rho = 1$ g cm^3 and $P_b = 10^6$ dynes/cm^2 (or 10^5 Pa), we find $kR = 0.01368$. Assuming that a bubble is excited by an incident sound wave of displacement amplitude A, then at resonance we can have $A/a \ll 1$, where a is the amplitude of bubble oscillations. From the linear theory it is well known that, owing to radiation damping which is of $O(kR)$†, the amplitude ratio at resonance is of the order

$$A/a = O(kR) \equiv O(\epsilon) \ll 1. \tag{2.3}$$

On the bubble surface the first-order oscillating quantities are characterized to be of $O(a/R)$ and the nonlinear effects of $O(a/R)^2$. In the incident sound the first-order

† For the bubble size of interest here, the radiation damping is of the same order of magnitude as the total damping.

perturbations are measured to be of $O(kA)$ and nonlinearity of $O(kA)^2$. The ratio of the two nonlinearities is very small:

$$\frac{(kA)^2}{(a/R)^2} = \left(\frac{A}{a}\right)^2 (kR)^2 = O(\epsilon^4) \ll 1. \tag{2.4}$$

Therefore we can ignore nonlinearity in the far field of sound while considering the nonlinearity on the bubble surface. The far field is sufficiently well described by the linear wave equation

$$\nabla^2 \Phi = \frac{1}{C^2}\frac{\partial^2 \Phi}{\partial t^2}, \tag{2.5}$$

where Φ is related to pressure and velocity by

$$p = -\rho \frac{\partial \Phi}{\partial t}, \quad v = \nabla \Phi. \tag{2.6}$$

3. Near field of the bubble

In the near field $r = O(R)$ water compressibility can be ignored with an error of $O(kR)$ in the solution to be obtained. The velocity potential, denoted by φ, is governed by

$$\nabla^2 \varphi = 0. \tag{3.1}$$

For bubble oscillations of small amplitude, $a/R \ll 1$, Longuet-Higgins (1989*a*) has expanded the kinematic and dynamic boundary conditions about the mean radius. In the case of axial symmetry he gives, with second-order $(a/R)^2$ accuracy

$$\eta_t - \varphi_r = \eta\varphi_{rr} - \frac{1}{R^2}(\eta_\theta \varphi_\theta) \quad (r = R), \tag{3.2}$$

$$\varphi_t + \frac{T}{\rho R^2}(2+\nabla_s^2)\,\eta - R\omega_0^2\,\bar{\eta} = -\eta\varphi_{rt} - \tfrac{1}{2}(\nabla\varphi)^2 + \frac{T}{\rho R^3}2\eta(1+\nabla_s^2)\,\eta + \omega_0^2[\overline{\eta^2} - \tfrac{3}{2}(\gamma+1)\,\bar{\eta}^2] \quad (r = R), \tag{3.3}$$

where η denotes the radial displacement of the bubble surface from equilibrium, T is the surface tension coefficient and ∇_s^2 is the surface Laplacian:

$$\nabla_s^2 f \equiv \frac{1}{\sin\theta}\frac{\partial}{\partial\theta}\left(\sin\theta \frac{\partial f}{\partial \theta}\right). \tag{3.4}$$

The spherical average of η is defined by

$$\bar{\eta} = \frac{1}{4\pi}\int_0^{2\pi} \mathrm{d}\psi \int_0^{\pi} \eta(\theta,\psi)\sin\theta\,\mathrm{d}\theta = \frac{1}{2}\int_0^{\pi}\eta \sin\theta\,\mathrm{d}\theta \tag{3.5}$$

and ω_0 is given by (2.1). Gravity is neglected here.

Let

$$\eta = \epsilon\eta_1 + \epsilon^2\eta_2 + \ldots; \quad \varphi = \epsilon\varphi_1 + \epsilon^2\varphi_2 + \ldots. \tag{3.6}$$

The first-order approximation satisfies

$$\eta_{1t} - \varphi_{1r} = 0, \tag{3.7}$$

$$\varphi_{1t} + \frac{T}{\rho R^2}(2+\nabla_s^2)\,\eta_1 - R\omega_0^2\,\bar{\eta}_1 = 0. \tag{3.8}$$

A homogeneous solution satisfying (3.1), (3.7), and (3.8) may consists of an isotropic (breathing) mode and anisotropic modes with latitudinal distortion:

$$\eta_1 = a_0\,\mathrm{e}^{-\mathrm{i}\omega t} + a_n P_n(\cos\theta)\,\mathrm{e}^{-\mathrm{i}\sigma_n t} + *, \tag{3.9}$$

$$\varphi_1 = b_0 \frac{R}{r}\mathrm{e}^{-\mathrm{i}\omega t} + b_n \left(\frac{R}{r}\right)^{n+1} P_n(\cos\theta)\,\mathrm{e}^{-\mathrm{i}\sigma_n \tau} + * \tag{3.10}$$

where $*$ represents the complex conjugate of all preceding terms, $P_n(\cos\theta)$ is the Legendre polynomial of order n, and

$$b_0 = \mathrm{i}\omega R a_0, \quad b_n = \frac{\mathrm{i}\sigma_n R a_n}{n+1}. \tag{3.11 a, b}$$

The eigenfrequencies for these modes are given by

$$\omega^2 = \omega_0^2 - \frac{2T}{\rho R^3}, \quad \sigma_n^2 = (n-1)(n+1)(n+2)\frac{T}{\rho R^3} \tag{3.12 a, b}$$

(Lamb 1932). Although all modes $n = 2, 3, 4, \ldots$ can exist under general initial conditions, we shall first focus attention on the near-resonant interaction between the breathing mode and one of the distortion modes, say n, with ω and σ_n satisfying the following near-resonance condition:

$$\omega = 2\sigma_n + \Delta\omega_n \equiv 2\sigma_n + \epsilon\omega\lambda_n, \tag{3.13}$$

where $\Delta\omega_n \equiv \epsilon\omega\lambda_n$ denotes the frequency mismatch for the chosen R, with $\lambda_n \leqslant O(1)$. Extensions to more distortion modes will be discussed later. Expecting the modal amplitudes a_0, and a_n to vary slowly in time, we introduce the slow coordinate

$$t_1 = \epsilon t \tag{3.14}$$

in η_1 and φ_1 through a_0 and a_n in (3.9) and b_0 and b_n in (3.10). As a result the second-order solution must satisfy the following boundary conditions on the mean bubble surface:

$$\eta_{2t} - \varphi_{2r} = \eta_1\varphi_{1rr} - \frac{1}{R^2}\eta_{1\theta}\varphi_{1\theta} - \eta_{1t_1}, \tag{3.15}$$

$$\varphi_{2t} + \frac{T}{\rho R^2}(2+\nabla_s^2)\,\eta_2 - R\omega_0^2\,\overline{\eta}_2 = -\eta_1\varphi_{1rt} - \tfrac{1}{2}(\nabla\varphi_1)^2$$
$$+ \frac{T}{\rho R^2}(2\eta_1)(1+\nabla_s^2)\,\eta_1 + \omega_0^2[\overline{\eta_1^2} - \tfrac{3}{2}(\gamma+1)\,\overline{\eta}_1^2] - \varphi_{1t_1}, \tag{3.16}$$

which are taken from Longuet-Higgins (1989*a*) except for the last terms in (3.15) and in (3.16). The general second-order solution with axial symmetry about the polar axis can be formally written

$$\eta_2 = c_0 + \sum_{n=2} c_n P_n(\cos\theta), \tag{3.17}$$

$$\varphi_2 = d_0 \frac{R}{r} + \sum_{n=2} d_n \left(\frac{R}{r}\right)^{n+1} P_n(\cos\theta) + \bar{d}_0\,\mathrm{e}^{-\mathrm{i}\omega t} + *, \tag{3.18}$$

where c_0, c_n, d_0 and d_n are complex functions of t and t_1. The term $\bar{d}_0$ depends only on t_1 and is needed to match with the far field. Substituting (3.17) and (3.18) into (3.15), we get

$$\begin{aligned}
&\frac{\partial c_0}{\partial t}+\sum_{n=2}\frac{\partial c_n}{\partial t}P_n+\frac{1}{R}d_0+\sum_{n=2}(n+1)\frac{d_n}{R}P_n\\
&=\frac{2\mathrm{i}\omega}{R}(a_0^2\,\mathrm{e}^{-2\mathrm{i}\omega t}+a_0a_0^*)+\frac{2\mathrm{i}\omega}{R}(a_0a_n\,\mathrm{e}^{-\mathrm{i}(\omega+\sigma_n t}+a_0a_n^*\,\mathrm{e}^{-\mathrm{i}(\omega-\sigma_n)t})P_n\\
&+\mathrm{i}(n+2)\frac{\sigma_n}{R}(a_0a_n\,\mathrm{e}^{-\mathrm{i}(\sigma_n+\omega)t}-a_0a_n^*\,\mathrm{e}^{-\mathrm{i}(\omega-\sigma_n t)})P_n\\
&+(a_n^2\,\mathrm{e}^{-2\mathrm{i}\sigma_n t}+a_na_n^*)\left[\mathrm{i}(n+2)\frac{\sigma_n}{R}P_n^2-\frac{\mathrm{i}\sigma_n}{(n+1)R}\left(\frac{\mathrm{d}P_n}{\mathrm{d}\theta}\right)^2\right]\\
&-\left[\frac{\mathrm{d}a_0}{\mathrm{d}t_1}\mathrm{e}^{-\mathrm{i}\omega t}+\frac{\mathrm{d}a_n}{\mathrm{d}t_1}\mathrm{e}^{-\mathrm{i}\sigma_n t}P_n\right]+*. \qquad (3.19)
\end{aligned}$$

In order to facilitate the tracing of the origin of each term, simplification via (3.13) is postponed until later.

The spherical average of both sides of (3.19) gives

$$\frac{\partial c_0}{\partial t}+\frac{1}{R}d_0=\frac{2\mathrm{i}\omega}{R}(a_0^2\,\mathrm{e}^{-2\mathrm{i}\omega t}+a_0a_0^*)+\frac{2\mathrm{i}\sigma_n}{(2n+1)R}(a_n^2\,\mathrm{e}^{-2\mathrm{i}\sigma_n t}+a_na_n^*)-\frac{\mathrm{d}a_0}{\mathrm{d}t_1}\mathrm{e}^{-\mathrm{i}\omega t}+*. \qquad (3.20)$$

Next, multiplying (3.19) by $P_n(\cos\theta)$ and then taking the spherical average we get

$$\begin{aligned}
&\frac{1}{2n+1}\frac{\partial c_n}{\partial t}+\frac{n+1}{2n+1}\frac{d_n}{R}\\
&=\frac{\mathrm{i}[2\omega+(n+2)\sigma_n]}{(2n+1)R}a_0a_n\,\mathrm{e}^{-\mathrm{i}(\omega+\sigma_n)t}\\
&+\frac{\mathrm{i}}{R}\frac{2\omega-(n+2)\sigma_n}{2n+1}a_0a_n^*\,\mathrm{e}^{-\mathrm{i}(\omega-\sigma_n)t}-\frac{1}{2n+1}\frac{\mathrm{d}a_n}{\mathrm{d}t_1}\mathrm{e}^{-\mathrm{i}\sigma_n t}\\
&+(a_n^2\,\mathrm{e}^{-2\mathrm{i}\sigma_n t}+a_na_n^*)\left[\frac{\mathrm{i}}{R}(n+2)\sigma_n\overline{P_n^3}-\frac{\mathrm{i}\sigma_n}{(n+1)R}\overline{\left(\frac{\mathrm{d}P_n}{\mathrm{d}\theta}\right)^2P_n}\right]+*. \qquad (3.21)
\end{aligned}$$

Use has been made of the following identities:

$$\left.\begin{aligned}
&\bar{P}_n=\frac{1}{2}\int_0^\pi P_n(\cos\theta)\sin\theta\,\mathrm{d}\theta=0\\
&\overline{P_mP_n}=\begin{cases}0 & \text{if}\quad m\neq n,\\ \dfrac{1}{2n+1} & \text{if}\quad m=n;\end{cases}\\
&\overline{\frac{\mathrm{d}P_m}{\mathrm{d}\theta}\frac{\mathrm{d}P_n}{\mathrm{d}\theta}}=\begin{cases}0 & \text{if}\quad m\neq n,\\ \dfrac{m(m+1)}{2m+1} & \text{if}\quad m=n;\end{cases}\\
&\nabla_s^2P_n=-n(n+1)P_n,\quad \overline{\nabla_s^2\eta_2}=\nabla_s^2\bar{\eta}_2=0.
\end{aligned}\right\} \qquad (3.22)$$

Similar but lengthier treatment of (3.16) gives

$$\frac{\partial d_0}{\partial t}-R\omega^2 c_0 = \omega^2(a_0^2\,e^{-2i\omega t}+a_0\,a_0^*)+\frac{\sigma_n^2}{2n+1}(a_n^2\,e^{-2i\sigma_n t}+a_n a_n^*)$$

$$+\frac{\omega^2}{2}(a_0^2\,e^{-2i\omega t}-a_0\,a_0^*)+\frac{\sigma_n^2}{2(n+1)}(a_n^2\,e^{-2i\sigma_n t}-a_n\,a_n^*)$$

$$+\frac{2T}{\rho R^3}\left[(a_0^2\,e^{-2i\omega t}+a_0\,a_0^*)+\frac{1-n-n^2}{2n+1}(a_n^2\,e^{-2i\sigma_n t}+a_n\,a_n^*)\right]$$

$$+\omega_0^2\left[-\frac{3\gamma+1}{2}(a_0^2\,e^{-2i\omega t}+a_0\,a_0^*)+\frac{1}{2n+1}(a_n^2\,e^{-2i\sigma_n t}+a_n\,a_n^*)\right]$$

$$-iR\omega\frac{da_0}{dt_1}e^{-i\omega t}+i\omega\bar{d}_0\,e^{-i\omega t}+*, \tag{3.23}$$

and

$$\frac{1}{2n+1}\frac{\partial d_n}{\partial t}-\frac{2T}{\rho R^2}\frac{(n-1)(n+2)}{2(2n+1)}c_n$$

$$= a_0\,a_n\,e^{-i(\omega+\sigma_n)t}\left[\frac{\omega^2+\sigma_n^2}{2n+1}-\frac{(n-1)(n+2)(\omega_0^2-\omega^2)}{2n+1}+\frac{\omega\sigma_n}{2n+1}\right]$$

$$+\frac{1}{2n+1}a_0\,a_n^*\,e^{-i(\omega-\sigma_n)t}\left[\omega^2+\tfrac{1}{2}(n-1)^2(n+2)(\omega_0^2-\omega^2)-\omega\sigma_n\right]$$

$$+(a_n^2\,e^{-2i\sigma_n t}+a_n\,a_n^*)\left[\sigma_n^2+(1-n-n^2)(\omega_0^2-\omega^2)\right]\overline{P_n^3}$$

$$+\left[\frac{\sigma_n^2}{2(n+1)^2}\overline{\left(\frac{dP_n}{d\theta}\right)^2 P_n}+\frac{\sigma_n^2}{2}\overline{P_n^3}\right](a_n^2\,e^{-2i\sigma_n t}-a_n\,a_n^*)$$

$$-\frac{iR\sigma_n}{(n+1)(2n+1)}\frac{da_n}{dt_1}e^{-i\sigma_n t}+*. \tag{3.24}$$

Eliminating d_0 from (3.20) and (3.23), we get

$$\frac{\partial^2 c_0}{\partial t^2}+\omega^2 c_0 = \times\left[\frac{4\sigma_n^2}{(2n+1)R}-\frac{(n-1)(n+2)(4n-1)}{4(2n+1)R}(\omega_0^2-\omega^2)-\frac{\omega^2}{(2n+1)R}\right]a_n^2\,e^{-2i\sigma_n t}$$

$$+\left(2i\omega\frac{da_0}{dt_1}-\frac{i\omega}{R}\bar{d}_0\right)e^{-i\omega t}+\text{NST}+*, \tag{3.25}$$

where NST stands for non-secular terms which are not proportional to $\exp(\pm i\omega t)$ or $\exp(\pm 2i\sigma_n t)$. For uniform validity in t we require the secular terms to vanish, i.e.

$$i\sigma_n\frac{(4n-1)}{(n+1)(2n+1)}a_n^2\,e^{i\omega\lambda_n t_1}+8R\frac{da_0}{dt_1}-4\bar{d}_0 = 0, \tag{3.26}$$

where the quantity in the square brackets in (3.25) has been simplified with the aid of (3.12) and (3.13). The same conclusion is reached if c_0 is eliminated from (3.20) and (3.23) instead.

Similarly by eliminating d_n from (3.21) and (3.24), we get

$$\frac{1}{2n+1}\left(\frac{\partial^2 c_n}{\partial t^2}+\sigma_n^2 c_n\right) = (\omega-\sigma_n)\,[2\omega-(n+2)\,\sigma_n]\frac{1}{(2n+1)\,R}a_0\, a_n^* \,\mathrm{e}^{-\mathrm{i}(\omega-\sigma_n)t}$$

$$+\frac{2\mathrm{i}\sigma_n}{2n+1}\frac{\mathrm{d}a_n}{\mathrm{d}t}\mathrm{e}^{-\mathrm{i}\sigma_n t}-\frac{n+1}{(2n+1)\,R}[\omega^2+\sigma_n^2-\omega\sigma_n$$

$$-(n-1)\,(n+2)\,(\omega_0^2-\omega^2)]\,a_0\,a_n^*\,\mathrm{e}^{-\mathrm{i}(\omega-\sigma_n)t}+\mathrm{NST}+*. \tag{3.27}$$

Removal of secular forcing terms leads to

$$(4n-1)\,\mathrm{i}\sigma_n\,a_0\,a_n^*\,\mathrm{e}^{-\mathrm{i}\omega\lambda_n t_1}+2R\frac{\mathrm{d}a_n}{\mathrm{d}t_1} = 0. \tag{3.28}$$

Equations (3.26) and (3.28) describe the evolution of the complex amplitudes a_0 and a_n:

$$\frac{\mathrm{d}a_0}{\mathrm{d}t_1} = -\mathrm{i}Q_0^n\,a_n^2\,\mathrm{e}^{\mathrm{i}\omega\lambda_n t_1}+\frac{\bar{d}_0}{2R}, \tag{3.29}$$

$$\frac{\mathrm{d}a_n}{\mathrm{d}t_1} = -\mathrm{i}Q_n\,a_0\,a_n^*\,\mathrm{e}^{-\mathrm{i}\omega\lambda_n t_1}, \tag{3.30}$$

where

$$Q_0^n = \frac{(4n-1)\,\sigma_n}{8(n+1)\,(2n+1)\,R},\quad Q_n = \frac{(4n-1)\,\sigma_n}{2R}. \tag{3.31}$$

The coefficient $\bar{d}_0$ remains to be found by matching with the far-field solution. Note that the near-field solution up to the first two orders is

$$\varphi = \epsilon\left[b_0\frac{R}{r}\mathrm{e}^{-\mathrm{i}\omega t}+b_n\left(\frac{R}{r}\right)^{n+1}P_n(\cos\theta)\,\mathrm{e}^{-\mathrm{i}\sigma_n t}\right]$$

$$+\epsilon^2\left[d_0\frac{R}{r}+\sum_{m=2} d_m\left(\frac{R}{r}\right)^{m+1}P_m(\cos\theta)+\bar{d}_0\,\mathrm{e}^{-\mathrm{i}\omega t}\right]+*, \tag{3.32}$$

where b_0 and b_n are given by (3.11).

4. Evolution equations

The sound wave potential in the far field can be written

$$\Phi = \epsilon\Phi_1+\epsilon^2\Phi_2 = \epsilon B_0\frac{1}{kr}\mathrm{e}^{\mathrm{i}(kr-\omega t)}+\epsilon B_n P_n\,h_n(k_n\,r)\,\mathrm{e}^{\mathrm{i}k_n r-\mathrm{i}\sigma_n t}$$

$$+\epsilon^2\frac{\mathrm{i}p_0}{\rho\omega}\mathrm{e}^{(\mathrm{i}kx-\mathrm{i}\omega t)}+\ldots+*, \tag{4.1}$$

where $k_n = \sigma_n/C$, and h_n denotes the spherical Hankel function of the first kind corresponding to radiated waves. The coefficients B_0 and B_n are allowed to contain $O(\epsilon)$ and $O(\epsilon^2)$ terms. A plane incident wave with pressure amplitude p_0 and the frequency close to that of the breathing mode is included. Since the bubble is near resonance, we have assumed the incident wave to be at most of order $O(\epsilon^2)$.

We now require that the near and far fields be asymptotically matched up to $O(\epsilon^2)$:

$$\lim_{r/R \gg 1} (\epsilon\varphi_1 + \epsilon^2\varphi_2) = \lim_{kr/R \ll 1} (\epsilon\Phi_1 + \epsilon^2\Phi_2). \tag{4.2}$$

Matching (3.32) and (4.1), we obtain

$$\epsilon\left[b_0\frac{R}{r}\mathrm{e}^{-\mathrm{i}\omega t} + b_n\left(\frac{R}{r}\right)^{n+1} P_n\,\mathrm{e}^{-\mathrm{i}\sigma_n t}\right] + \epsilon^2\left[d_0\frac{R}{r} + \sum_{m=2} d_m\left(\frac{R}{r}\right)^{m+1} P_m + \bar{d}_0\,\mathrm{e}^{-\mathrm{i}\omega t}\right] + *$$

$$= \epsilon\left[B_0\frac{1}{kr}(1+\mathrm{i}kr)\,\mathrm{e}^{-\mathrm{i}\omega t} - \sum_{m=2} B_n P_n\frac{(2n-1)\,!!}{(k_n r)^{n+1}}\mathrm{e}^{-\mathrm{i}\sigma_n t}\right] + \epsilon^2\frac{\mathrm{i}p_0}{\rho\omega}\mathrm{e}^{-\mathrm{i}\omega t} + *. \tag{4.3}$$

Since for small $k_n r$

$$h_n(k_n r) \approx -\mathrm{i}\frac{(2n-1)\,!!}{(k_n r)^{n+1}}, \quad \text{where} \quad (2n-1)\,!! = 1\times 3\times 5\ldots(2n-1), \tag{4.4}$$

it follows that

$$b_0 = \frac{B_0}{kR} = \mathrm{i}\omega R a_0 \quad \text{or} \quad B_0 = \mathrm{i}\omega kR\,Ra_0 = O(\epsilon), \tag{4.5a}$$

$$b_n = -B_n\frac{(2n-1)\,!!}{(k_n R)^{n+1}} \quad \text{or} \quad B_n = O(\epsilon^{n+1}), \tag{4.5b}$$

$$\bar{d}_0 = -\left(\frac{kR}{\epsilon}\right)\omega R a_0 + \frac{\mathrm{i}p_0}{\rho\omega}. \tag{4.5c}$$

Note from (4.5) that $B_0 = O(\epsilon)\,b_0$ and $B_n = O(k_n R)^{n+1}\,b_n$ for $n = 2, 3, \ldots$. This means that sound radiated from the bubble is only of $O(\epsilon^2)$, arising mainly from the breathing mode.

With (4.5c) we finally obtain from (3.29) and (3.30) the evolution equations for a_0 and a_n:

$$\frac{\mathrm{d}a_0}{\mathrm{d}t_1} = -\mathrm{i}Q_0^n\,a_n^2\,\mathrm{e}^{\mathrm{i}\omega\lambda_n t_1} - \tfrac{1}{2}\frac{kR}{\epsilon}\omega a_0 + \frac{\mathrm{i}f_0}{2\rho\omega R}\mathrm{e}^{\mathrm{i}\omega\Omega t_1}, \tag{4.6}$$

$$\frac{\mathrm{d}a_n}{\mathrm{d}t_1} = -\mathrm{i}Q_n\,a_0\,a_n^*\,\mathrm{e}^{-\mathrm{i}\omega\lambda_n t_1}, \tag{4.7}$$

where a frequency detuning is allowed in p_0,

$$p_0 = f_0\,\mathrm{e}^{\mathrm{i}\Delta\omega_f t} = f_0\,\mathrm{e}^{\mathrm{i}\omega\Omega t_1} \tag{4.8}$$

with $\Delta\omega_f \equiv \epsilon\omega\Omega$ and f_0 is a complex constant. The second term on the right-hand side of (4.6) represents radiation damping. This pair of equations describe the forced resonant interaction of the breathing and distortion mode in a perfect fluid. Note that while quadratic terms are involved, this theory is concerned with the evolution of first-order amplitudes over a long time $t_1 = (\epsilon/\omega T_0)\,\omega t = O(1)$.

In view of (3.31), $Q_0^n \sim \sigma_n/4nR$ is small while $Q_n \sim 2n\sigma_n/R$ is large for large n. Thus a_n must be large to affect a_0, while a small a_0 can affect a_n. It can be shown by repeating the matching argument that a plane incident wave at frequency $\sigma_n \approx \frac{1}{2}\omega$ has no effect on these evolution equations at the present order of approximation, i.e. the distortion mode cannot be excited directly by the incident wave.

In real fluids additional damping can be contributed by viscosity and by thermal diffusion in the air inside the bubble. A detailed account of the viscous damping by the nth mode was given by Longuet-Higgins (1989*b*, equation 4.15). Let us define the radiation damping constant which is non-zero for the breathing mode,

$$\gamma_R = \tfrac{1}{2}\omega kR. \tag{4.9}$$

The viscous damping, estimated by a linear analysis, gives rise to the damping constant

$$\gamma_{vn} = \frac{(n+2)(2n+1)\nu}{R^2} \tag{4.10}$$

for the nth distortion mode, and

$$\gamma_{v0} = \frac{2\nu}{R^2} \tag{4.11}$$

for the breathing mode. As pointed out by Longuet-Higgins (1989*b*), (4.10) gives only an order-of-magnitude estimate, as the effective Stokes boundary-layer thickness is, for large enough n, not necessarily small compared to the bubble radius, as is required by the approximation leading to (4.10).

Damping due to thermal diffusion affects the breathing mode and has been estimated by

$$\gamma_{th} = \frac{\omega}{2}\frac{3(\gamma-1)}{2R}\left(\frac{2D}{\omega}\right)^{\frac{1}{2}} \tag{4.12}$$

(Pfriem 1940, see van Wijngaarden 1972), where $D = 0.2\ \mathrm{cm^2/s}$ is the thermal diffusivity in air. This corresponds to Eller's (1970) formula $(2D/\omega)^{\frac{1}{2}}/R \ll 1$ (see van Wijngaarten 1980). A more detailed theory for isotropic oscillations has been given by Prosperetti (1977) who showed that at resonance, the damping factors due to radiation and to diffusion are nearly the same, while viscous effects are insignificant for a radius in the range of $O(10^{-2})\ \mathrm{cm} < R < O(1)\ \mathrm{cm}$.

To account for all these points, we modify (4.6) and (4.7) to

$$\frac{\mathrm{d}a_0}{\mathrm{d}t_1} = -\mathrm{i}Q_0^n\, a_n^2\, \mathrm{e}^{\mathrm{i}\omega\lambda_n t_1} - \frac{\gamma_0}{\epsilon}a_0 + \frac{\mathrm{i}f_0}{2\rho\omega R}\mathrm{e}^{\mathrm{i}\omega\Omega t_1}, \tag{4.13}$$

$$\frac{\mathrm{d}a_n}{\mathrm{d}t_1} = -\mathrm{i}Q_n\, a_0\, a_n^*\, \mathrm{e}^{-\mathrm{i}\omega\lambda_n t_1} - \frac{\gamma_n}{\epsilon}\alpha_n, \tag{4.14}$$

where

$$\gamma_0 = \tfrac{1}{2}kR\omega + \frac{2\nu}{R^2} + \frac{3(\gamma-1)}{4}\frac{\omega}{R}\left(\frac{2D}{\omega}\right)^{\frac{1}{2}}, \tag{4.15}$$

$$\gamma_n = (n+2)(2n+1)\frac{\nu}{R^2}. \tag{4.16}$$

If forcing due to the incident wave is absent, (4.13) and (4.14) are familiar in nonlinear optics where they describe the *second harmonic generation* of light of frequency $2\sigma_n$ when incident light of high intensity and frequency σ_n shines through a quartz crystal (Armstrong *et al.* 1962). They also arise in the theory of long waves in shallow water (see Mei & Ünlüata 1972 or Mei 1989). If dissipation is also ignored, it is known that when both modes are initially non-zero, their energy can be exchanged periodically in time. If the second harmonic ($\omega = 2\sigma_n$) is initially zero, then it can grow by draining energy completely from the first harmonic (σ_n).

Equations (4.13) and (4.14) are limited to two interacting modes. As is evident from (3.12*b*), the distortion modes are quite dense in the (σ_n, R)-diagram. In particular, the frequency separation between adjacent modes,

$$\sigma_{n+1} - \sigma_n \approx 3/n2\sigma_n \approx 3/n\omega, \tag{4.17}$$

can be as small as the resonance mismatch $\epsilon\omega\lambda_n$ for large enough n. Therefore for a sufficiently large bubble the isotropic mode can interact nearly resonantly with not only the distortion mode with the closest $2\sigma_n$, but one or several of its neighbours. Since the distortion modes do not interact directly among one another, the evolution equations can be easily modified to

$$\left.\begin{aligned}\frac{\mathrm{d}a_0}{\mathrm{d}t_1} &= -\frac{\gamma_0}{\epsilon} - \mathrm{i}\sum_m Q_0^m a_m^2 \,\mathrm{e}^{\mathrm{i}\omega\lambda_m t_1} + \frac{\mathrm{i}f_0}{2\rho\omega R}\mathrm{e}^{\mathrm{i}\omega\Omega t_1}, &(4.18)\\ \frac{\mathrm{d}a_m}{\mathrm{d}t_1} &= -\frac{\gamma_m}{\epsilon}a_m - \mathrm{i}Q_m a_0 a_m^* \,\mathrm{e}^{-\mathrm{i}\omega\lambda_m t_1}, &(4.19)\end{aligned}\right\} \quad m = n, n\pm 1, \ldots,$$

where m denotes the distortion modes satisfying the near-resonance condition.

Note however that a distortion mode must have non-zero initial value for it to take part in the resonant interaction. It is instructive and theoretically legitimate to first single out one such mode, and assume that all other neighbouring modes are initially absent. We therefore return to (4.13) and (4.14) for just one distortion mode, and introduce the timescale

$$T_0 = \left(\frac{2\rho\omega R}{|f_0|Q_n}\right)^{\frac{1}{2}}, \tag{4.20}$$

where $\epsilon^2|f_0|$ is the amplitude of the incident sound pressure, and the following scaled variables:

$$\tau = t_1/T_0, \quad \tilde{A}_0 = (T_0 Q_n)\, a_0, \quad \tilde{A}_n = [T_0(Q_0^n Q_n)^{\frac{1}{2}}]\, a_n. \tag{4.21}$$

Equations (4.13) and (4.14) then become

$$\frac{\mathrm{d}\tilde{A}_0}{\mathrm{d}\tau} = -\alpha_0 \tilde{A}_0 - \mathrm{i}\tilde{A}_n^2 \,\mathrm{e}^{\mathrm{i}\tilde{\lambda}_n\tau} + \mathrm{i}F\,\mathrm{e}^{\mathrm{i}\tilde{\Omega}\tau}, \tag{4.22}$$

$$\frac{\mathrm{d}\tilde{A}_n}{\mathrm{d}\tau} = -\mathrm{i}\tilde{A}_0 \tilde{A}_n^* \,\mathrm{e}^{-\mathrm{i}\tilde{\lambda}_n\tau} - \alpha_n \tilde{A}_n, \tag{4.23}$$

where F is the normalized amplitude of the far-field pressure, and a complex number of unit magnitude. The other dimensionless parameters are

$$\left.\begin{aligned}\alpha_0 &= \frac{\gamma_0}{\omega}\frac{\omega T_0}{\epsilon}, \quad \alpha_n = \frac{\gamma_n}{\omega}\frac{\omega T_0}{\epsilon},\\ \tilde{\Omega} = \Omega(\omega T_0) &= \frac{\Delta\omega_{\mathrm{f}}}{\omega}\frac{\omega T_0}{\epsilon}, \quad \tilde{\lambda}_n = \lambda_n(\omega T_0) = \frac{\Delta\omega_n}{\omega}\frac{\omega T_0}{\epsilon}.\end{aligned}\right\} \tag{4.24}$$

For a fixed bubble of radius R near the sea surface, the values of damping constants γ_0/ω, γ_n/ω and the phase mismatch $\Delta\omega_n/\omega$ are fixed for a chosen modal number n. The effects of varying the forcing are through the detuning frequency $\Delta\omega_{\mathrm{f}}/\omega$ and the amplitude parameter ϵ/T_0.

R(cm)	n	α_0	α_n	$\tilde{\lambda}_n$	Ω_-	Ω_+
0.01	3	0.136382	0.171	4.645	0.014	0.452
	4		0.264	1.968	0.049	0.820
	5		0.376	−0.974	—	—
	6		0.508	−4.167	−0.49	−0.04
0.1	9	0.1366	0.1098	1.719	0.03	0.771
	10		0.123	1.591	0.035	0.714
	11		0.1459	−0.556	—	—
	12		0.1788	−1.523	−0.67	−0.04
	13		0.1976	−3.416	−0.69	−0.02
1.0	21	0.1366	0.0483	1.5	0.022	0.700
	22		0.0527	0.898	0.041	0.402
	23		0.0573	0.29	—	—
	24		0.0622	−0.83	−0.361	−0.04
	25		0.0672	−0.97	−0.434	−0.04

TABLE 1. Coupling coefficients and Hopf bifurcation points

In table 1 we list these parameters for several modes and for $R = 0.01$, 0.1 and 1 cm, calculated on the basis that $\epsilon/\omega T_0 = 0.1$.

Finally we convert the system (4.22) and (4.23) to an autonomous one by the transformation

$$\tilde{A}_0 = A_0 e^{i\tilde{\Omega}\tau}, \quad \tilde{A}_n = A_n e^{\frac{1}{2}i(\tilde{\Omega}-\tilde{\lambda}_n)\tau}, \tag{4.25}$$

yielding

$$\frac{dA_0}{d\tau} = -i\beta_0 A_0 - \alpha_0 A_0 - iA_n^2 + iF, \tag{4.26}$$

$$\frac{dA_n}{dt} = -i\beta_n A_n - \alpha_n A_n - iA_0 A_n^*, \tag{4.27}$$

where

$$\beta_0 = \tilde{\Omega}, \quad \beta_n = \tfrac{1}{2}(\tilde{\Omega} - \tilde{\lambda}_n). \tag{4.28}$$

Note from (4.21) and (3.31) that the scale of a_0 decreases with n for large n, while that of a_n does not. It is in this normalized sense that the two modes are said to be comparable.

Let us rewrite (4.26) and (4.27) in Cartesian form by letting

$$A_0 = C_0 + iS_0, \quad A_n = C_n + iS_n, \tag{4.29}$$

then

$$\frac{dC_0}{d\tau} = -\alpha_0 C_0 + \beta_0 S_0 + 2C_n S_n - q, \tag{4.30}$$

$$\frac{dS_0}{d\tau} = -\beta_0 C_0 - \alpha_0 S_0 - (C_n^2 - S_n^2) + p, \tag{4.31}$$

$$\frac{dC_n}{d\tau} = -\alpha_n C_n + \beta_n S_n + (S_0 C_n - C_0 S_n), \tag{4.32}$$

$$\frac{dS_n}{d\tau} = -\alpha_n S_n - \beta_n C_n - C_0 C_n - S_0 S_n. \tag{4.33}$$

This is the same autonomous system as discussed by Miles (1984) whose analysis for a special case ($\alpha_n = \alpha_0 = \alpha$, $\beta_n = \frac{1}{2}\beta_0 = \beta$, i.e. $\tilde{\lambda}_n \equiv 0$) did not yield any chaotic response. For capillary–gravity waves in a vertically oscillating tank, Gu & Sethna

(1987) deduced a similar set of equations without forcing and found a variety of chaotic responses if the above restrictions are removed. Since in nature finite phase mismatch most likely occurs, we shall relax Miles' instability analysis and allow imperfect resonance. For simplicity we also assume $q = 0$ so that $F = p + \mathrm{i}q = 1$ from here on.

The amplitude evolution equations (4.30)–(4.33) are deduced for the same time range $\tau = \epsilon\omega t = O(1)$. Because this is also the timescale of damping, the solution is expected to approach an asymptotic state (the attractor) at the end of this time range. While a higher-order theory can in principle extend the time range of validity, little substantive change is expected in the asymptotic state, according to the centre manifold theorem (Carr 1981; Rand & Armbruster 1987). Hence this type of low-order evolution equation, which can be derived by a variety of means (multiple-scale expansion (Miles 1984), method of averaging (Gu & Sethna 1987) or centre manifold and normal form theories (Meron & Procaccia 1986)), has been the customary basis for numerical computations for the asymptotic states (limit cycles, tori and chaos). In the case of standing waves in a tank, such theories have been found to agree with experiments reasonably well (Meron & Procaccia 1986; Simonelli & Gollub 1989; Kambe & Umedi 1990).

5. Fixed points and linearized instability for two-mode interaction

For the dynamical system (4.30)–(4.33) there are two fixed points. The first $\{X_j^{(1)}\}$ is at

$$\{X_j^{(1)}\}: \quad \bar{C}_0 = \frac{\beta_0}{\alpha_0^2+\beta_0^2}, \quad \bar{S}_0 = \frac{\alpha_0}{\alpha_0^2+\beta_0^2}, \quad \bar{C}_n = \bar{S}_n = 0. \tag{5.1}$$

Physically, this is an equilibrium state where the external forcing on the breathing mode is balanced by damping, while the distortion mode is at rest. As was shown by Miles, infinitesimal disturbances (C_0', S_0') and (C_n', S_n') are uncoupled. The disturbance of the breathing mode is always stable while that of the distortion mode n is

$$\begin{matrix}\text{stable}\\ \text{unstable}\end{matrix} \quad \text{if} \quad (\alpha_0^2+\beta_0^2)(\alpha_n^2+\beta_n^2) \gtrless 1. \tag{5.2}$$

The second fixed point $\{X_j^{(2)}\}$ can be conveniently expressed in polar form

$$\bar{C}_0 + \mathrm{i}\bar{S}_0 = \rho_0\,\mathrm{e}^{\mathrm{i}\theta_0}, \quad \bar{C}_n + \mathrm{i}\bar{S}_n = \rho_n\,\mathrm{e}^{\mathrm{i}\theta_n}; \tag{5.3}$$

then

$$\left.\begin{aligned} \rho_0 &= (\alpha_n^2+\beta_n^2)^{\frac{1}{2}}, \\ \cos\theta_0 &= (\beta_0\rho_0^2 - \beta_n\rho_n^2)/\rho_0, \quad \sin\theta_0 = (\alpha_0\rho_0^2+\alpha_n\rho_n^2)/\rho_0, \\ \rho_n &= \{-\alpha_0\alpha_n + \beta_0\beta_n + [1-(\alpha_0\beta_n+\alpha_n\beta_0)^2]^{\frac{1}{2}}\}^{\frac{1}{2}}, \\ \cos 2\theta_n &= [1-(\alpha_0\beta_n+\alpha_n\beta_0)^2]^{\frac{1}{2}}, \quad \sin 2\theta_n = -a_0 b_n - \alpha_n\beta_0, \end{aligned}\right\} \tag{5.4}$$

The range of parameters will be chosen so that the square roots are real, then the positive branches are taken. The linearized stability of $\{X_j^{(2)}\}$ leads to the following eigenvalue problem:

$$J_4\lambda^4 + J_3\lambda^3 + J_2\lambda^2 + J_1\lambda + J_0 = 0, \tag{5.5}$$

where

$$\begin{aligned} J_0 &= 4(\bar{C}_n + \bar{S}_n)\,r > 0, \\ J_1 &= 4(\alpha_0+\alpha_n)(\bar{C}_n^2+\bar{S}_n^2) + 2\alpha_n(\alpha_0^2+\beta_0^2) > 0, \\ J_2 &= 4(\bar{C}_n^2+\bar{S}_n^2) + \alpha_0^2+\beta_0^2+4\alpha_0\alpha_n > 0, \\ J_3 &= 2(\alpha_0+\alpha_n) > 0, \\ J_4 &= 1, \end{aligned}$$

with $$r = [1-(\alpha_n\beta_0+\alpha_0\beta_n)^2]^{\frac{1}{2}}.$$

According to the Routh–Hurwicz criterion the linearized system near $\{X_j^{(2)}\}$ is stable if

$$J_0 > 0, \quad J_1 > 0, \quad J_3 J_4 > 0, \tag{5.6a–c}$$

and

$$P = J_1(J_2 J_3 - J_1 J_4) - J_0 J_3^2 > 0. \tag{5.6d}$$

The first three conditions are always satisfied. But the last, (5.6*d*), is not satisfied for certain parameter ranges. By calculating P *vs.* $\tilde{\Omega}$ for fixed R and n, we can find the range of instability $\Omega_- < \tilde{\Omega} < \Omega_+$. The threshold values of Ω_- and Ω_+ are listed also in table 1.

By taking $\tilde{\Omega}$ to be near either threshold we have calculated all four eigenvalues from (5.5) and found the thresholds to be Hopf bifurcation points. Although approximate analyses near them can be carried out in principle with considerable computations, we have chosen to integrate the nonlinear system directly, by an Adams–Bashforth scheme with error allowance equal to 10^{-9}. Only the phase portraits of C_0 *vs.* S_0 will be shown; all for very large τ when they have settled on the attractor. All power spectra are computed for C_0 with 8192 sampling points. Before describing these numerical experiments, we recall that the global behaviour of the system is an attractor since the Lie derivative of (4.30)–(4.33) is always negative (Miles 1984):

$$\frac{\partial \dot{X}_i}{\partial X_i} = -2(\alpha_0+\alpha_n) < 0 \quad \text{where} \quad \{X_i\} = \{C_0, S_0, C_n, S_n\}. \tag{5.7}$$

The following energy conservation law is also derivable from (4.26) and (4.27):

$$\frac{\mathrm{d}}{\mathrm{d}t}(|A_0|^2+|A_n|^2) = -2(\alpha_0|A_0|^2+\alpha_n|A_n|^2)+(\mathrm{i}FA_0^*+*). \tag{5.8}$$

Vanishing of the right-hand side defines an ellipsoid in the four-dimensional phase space of $\{X_j\}$:

$$\frac{1}{\alpha_0}[(C_0+\tfrac{1}{2}q)^2+(S_0-\tfrac{1}{2}p)^2]+1/\alpha_n(C_n^2+S_n^2) = 1/4\alpha_0. \tag{5.9}$$

Similar to Lorenz's (1963) reasoning on his attractor, on any hypersphere large enough to contain the above ellipsoid, all phase trajectories must be attracted inward.

6. Long-time interaction between two modes

We select for illustration a small bubble $R = 0.01$ cm. The breathing mode frequency ω lies between σ_4 and σ_5. Only the interaction between ω and $2\sigma_4$ is of interest, since there is a region of instability $0.049 < \tilde{\Omega} < 0.820$. Note that the other neighbouring modes are either stable ($n = 5$) or mismatched in phase by a large amount ($n = 3$) when interacting singly with the breathing mode. Leaving the case of multi-mode interactions until the next section, we consider ω and $2\sigma_4$ only.

The initial data are set to be $C_0 = S_0 = S_n = 0$, $C_n = 1.0$. When $\tilde{\Omega}$ is not in the range of instability, the flow is always attracted to the equilibrium point. Decreasing from Ω_+ we first get a limit cycle. Figure 1 shows a sample phase portrait (C_0, S_0) and

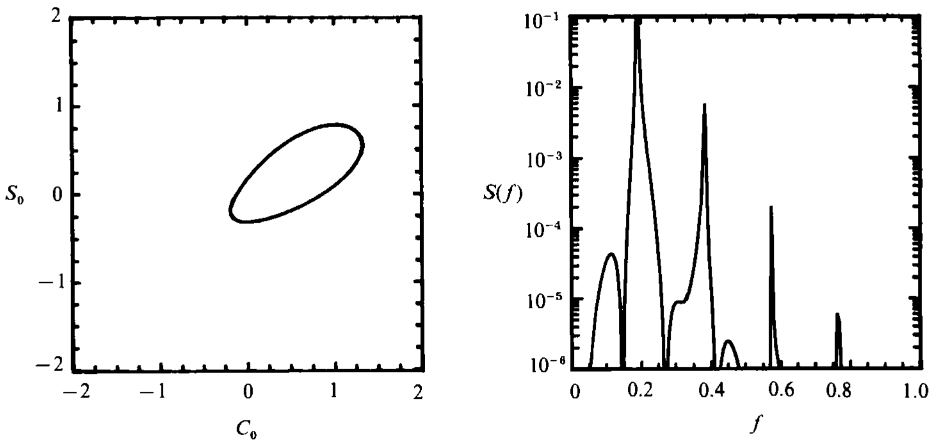

FIGURE 1. $\tilde{\Omega} = 0.750$, just below the upper Hopf bifurcation point.

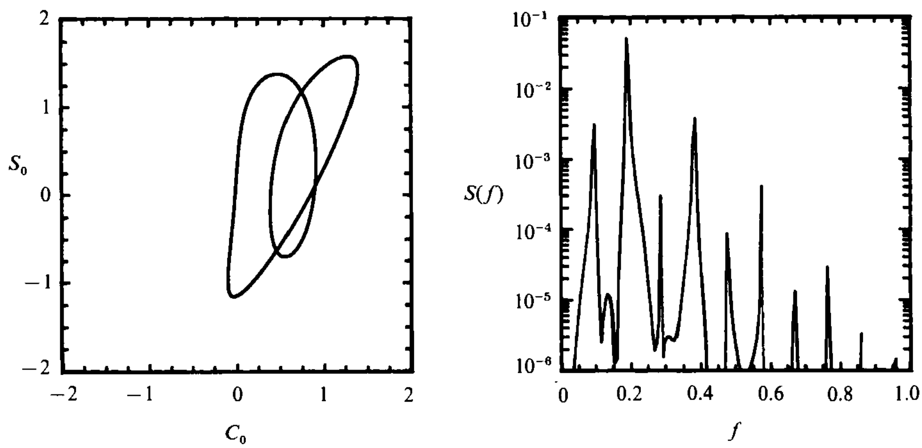

FIGURE 2. $\tilde{\Omega} = 0.410$, the threshold of period doubling.

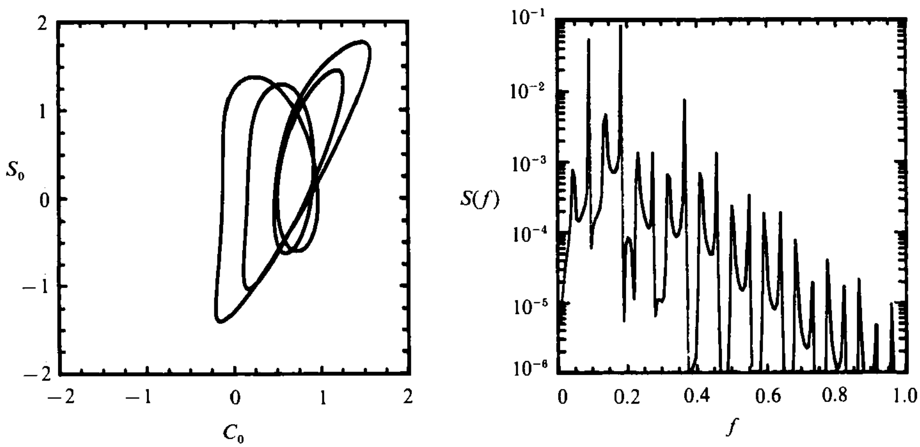

FIGURE 3. $\tilde{\Omega} = 0.371$, the threshold of period quadrupling.

the power spectrum of C_0 for $\tilde{\Omega} = 0.75$. At $\tilde{\Omega} = 0.41$, the first period-doubling appears, see figure 2. The second period-doubling occurs at $\tilde{\Omega} = 0.371$, see figure 3. The flow is chaotic in the range of $0.049 < \tilde{\Omega} < 0.360$ except for a narrow window which resides in $0.196 < \tilde{\Omega} < 0.20073$. A sample phase portrait and power spectrum

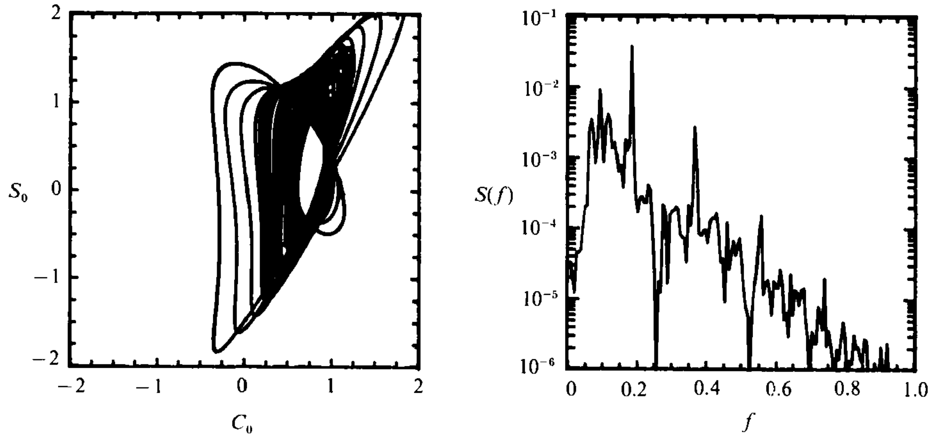

FIGURE 4. $\tilde{\Omega} = 0.300$, chaotic state.

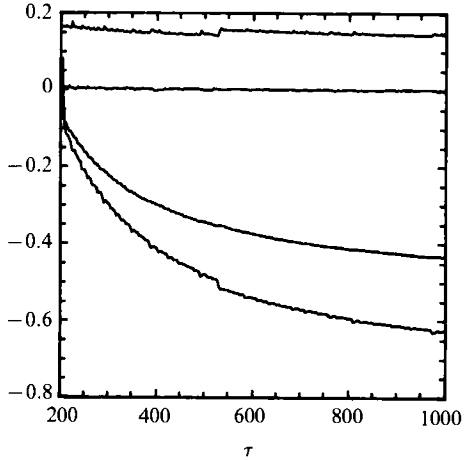

FIGURE 5. Lyaponov exponents *vs.* τ for $\tilde{\Omega} = 0.300$. The largest exponent is positive.

for $\tilde{\Omega} = 0.30$ are shown in figure 4. The asymptotic state corresponds to a strange attractor, as is evident by the Lyaponov exponents plotted in figure 5. For this case the Lyaponov dimension is 1.66 according to the definition by Kaplan & Yorke (1979). In the centre of the window the typical flow is a periodic state with fundamental frequencies 0.61, 1.22 and 1.83; its sample phase portrait and spectrum are shown in figure 6.

To see the flow near the lower boundary Ω_- we plot a time series of C_0 for $\Omega = 0.052$ in figure 7. Much of the time it is approximately periodic with slowly growing amplitude. After a long interval it bursts and collapses suddenly to a small amplitude, and then oscillates, again with slow amplification. This intermittent sequence of slowly amplifying oscillations and sudden bursts is erratic. The closer $\tilde{\Omega}$ is to Ω_-, the longer the separation between bursts becomes.

The general pattern of bifurcations and chaos remains the same for other R and n as long as just one distortion mode interacts with the breathing mode.

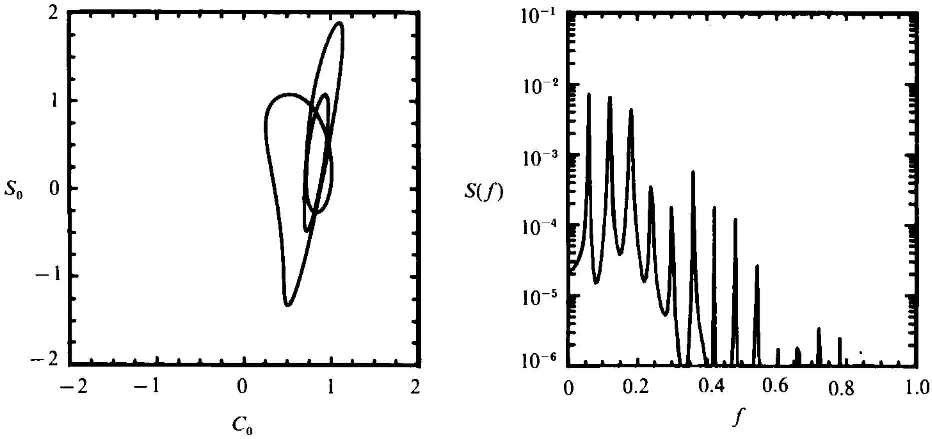

FIGURE 6. Periodic state in a window.

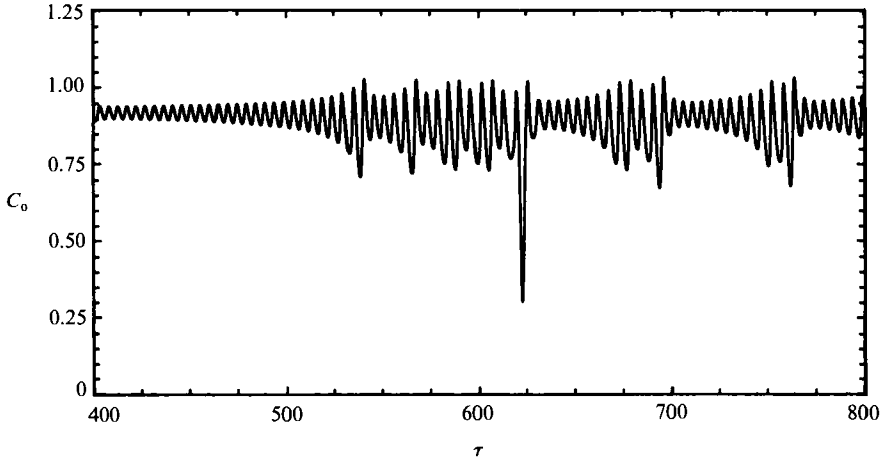

FIGURE 7. Time series for C_0 at $\tilde{\Omega} = 0.052$, very near the lower Hopf bifurcation point.

7. Long-time interaction between three modes

To examine a more complex and less idealized case, we consider a larger bubble with $R = 0.1$ cm and allow two distortion modes to have non-zero initial values. The two modes will then be expected to interact with each other indirectly through the breathing mode. It is interesting to see when and how bifurcations of the three-mode system evolve.

Using (4.21) and defining further:

$$A_m = a_m/T(Q_n Q_0^n)^{\frac{1}{2}} = \tilde{A}_m \, e^{i(\tilde{\Omega}-\tilde{\lambda}_m)\tau/2}, \quad \tilde{\lambda}_m = \omega T \lambda_m,$$

we rewrite the evolution equations (4.18) and (4.19) as follows:

$$\frac{dA_0}{d\tau} = -\alpha_0 a_0 - i\tilde{\Omega} a_0 - iA_n^2 - iUA_m^* + iF, \tag{7.1}$$

$$\frac{dA_n}{d\tau} = -[\alpha_n + \tfrac{1}{2}i(\tilde{\Omega} - \tilde{\lambda}_n)]\, a_n - iA_0 A_n^*, \tag{7.2}$$

$$\frac{dA_m}{d\tau} = -[\alpha_m + \tfrac{1}{2}i(\tilde{\Omega} - \tilde{\lambda}_m)]\, a_m - iSA_0 A_m^*, \tag{7.3}$$

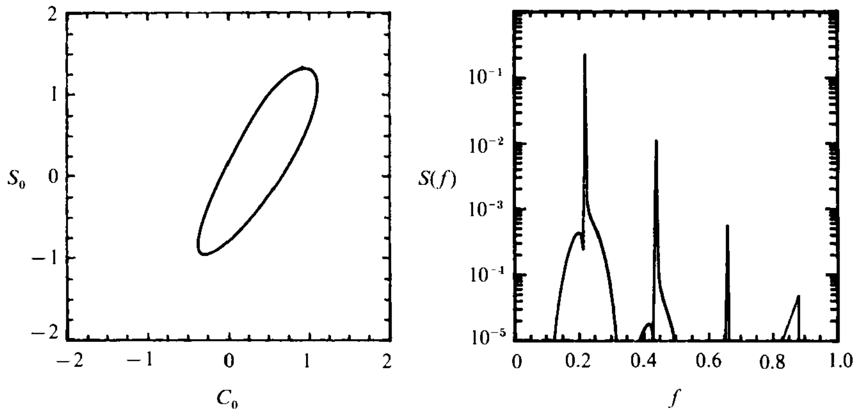

FIGURE 8. $\tilde{\Omega} = 0.600$, just below the upper Hopf bifurcation point.

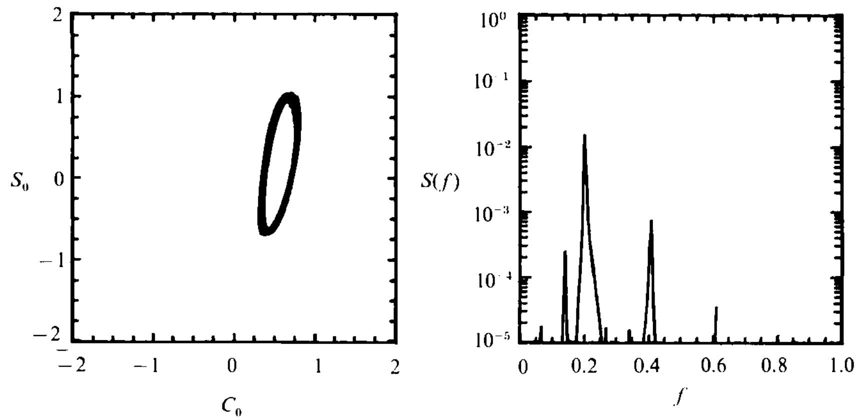

FIGURE 9. $\tilde{\Omega} = 0.360$, the threshold of quasi-periodic torus with two frequencies. Scales of phase portrait are distorted.

where
$$U = Q_0^m / Q_0^n, \quad S = Q_m / Q_n. \tag{7.4}$$

We omit the details of the fixed points and the linearized instability analysis, both of which would involve some numerical work. Instead we integrate the dynamical system with six real unknowns directly. By numerical experiments with all pairings of distortion modes for $R = 0.01$, 0.1 and 1 cm, we have found that unless their $\tilde{\Omega}$-ranges of two-mode instability, as listed in table 1, intersect, the flow is always attracted to an equilibrium state. Take $R = 0.1$ for example. There is no chaos if (n, m) is any of the following pairs: (9, 11), (9, 12), (9, 13), (10, 11), (10, 12), (10, 13). Only in the region of intersection can the three-mode interaction exhibit bifurcation and chaos.

We discuss below the results for $n = 10$, $m = n-1 = 9$ with equal initial values $A_0 = 0$, $A_n = A_m = 0.5$. It follows from (3.31) that $U = 0.727$ and $S = 0.88$, both of which are not far from unity. Crudely speaking on $\alpha_n \approx \alpha_m$, $\tilde{\lambda}_n \approx \tilde{\lambda}_m$ and R $\approx S \approx 1$; therefore the two neighbouring modes might be expected to have similar behaviour while A_0 would behave as if there were only one distortion mode A_n (or A_m) with the initial value 1.

The $\tilde{\Omega}$-domain of linearized instability for the two-mode system (0, 9) is 0.03 <

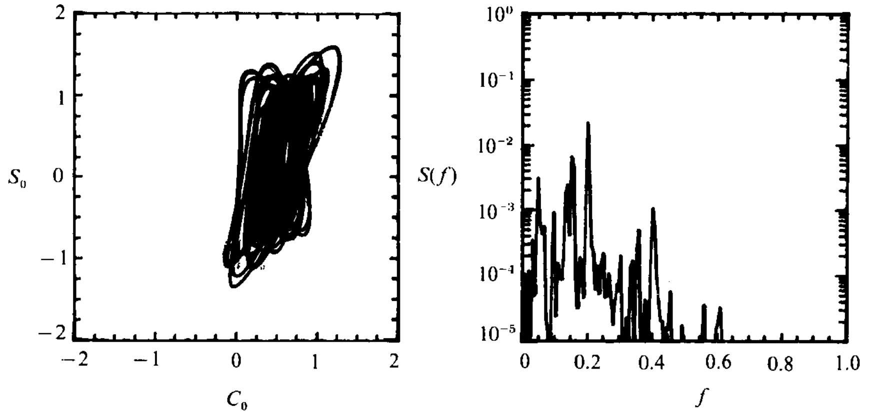

FIGURE 10. $\tilde{\Omega} = 0.35901$, threshold to chaos with three incommensurable periods.

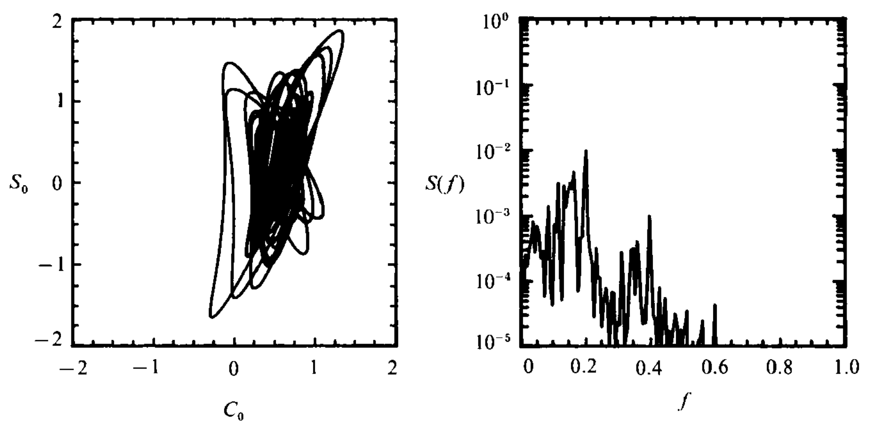

FIGURE 11. $\tilde{\Omega} = 0.3$, chaos.

$\tilde{\Omega} < 0.77$, which includes the instability region of the two-mode system (0, 10): $0.035 < \tilde{\Omega} < 0.714$.

As $\tilde{\Omega}$ is reduced below 0.714, a limit cycle appears. A typical phase portrait is shown for $\tilde{\Omega} = 0.600$ in figure 8. The dominant frequency is near $f = 0.201$. Near $\tilde{\Omega} = 0.36$ the limit cycle bifurcates to a quasi-periodic torus, which is characterized by two frequencies (0.14 and 0.201) whose ratio is not rational; the third frequency 0.402 is the second harmonic of 0.201. The phase trajectory in figure 9 fills a broadbanded circuit. At $\tilde{\Omega} = 0.35901$, the flow becomes chaotic, see figure 10. Note that the power spectrum shows three strong frequencies.

For the remainder of the range $0.035 < \tilde{\Omega} < 0.359$ the flow is chaotic. A sample case for $\tilde{\Omega} = 0.3$ is shown in figure 11. Also when $\tilde{\Omega}$ is close to $\Omega_- = 0.035$, the typical time series is a long stretch of amplifying oscillations followed by sudden burst, and then a long stretch of amplifying oscillations again, etc., see figure 12.

In summary, unlike the two-mode interaction where the path from Ω_+ to chaos is a Feingenbaum sequence of period-doublings, the case of the three-mode interactions belongs to the Ruelle–Takens class in that the limit cycle bifurcates first to a quasi-periodic torus and then to chaos (Berge, Pomeau & Vidal 1984). Qualitatively the same results are found for $R = 0.01$ and 1 cm.

Combined with the theory of Benjamin & Ellis (1990), our results for chaotic

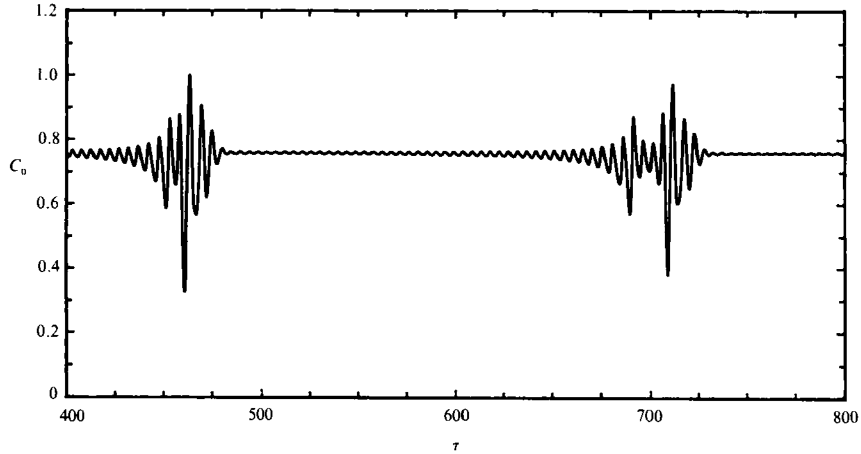

FIGURE 12. Time series of C_0 at $\tilde{\Omega} = 0.040$ near the lower Hopf bifurcation point.

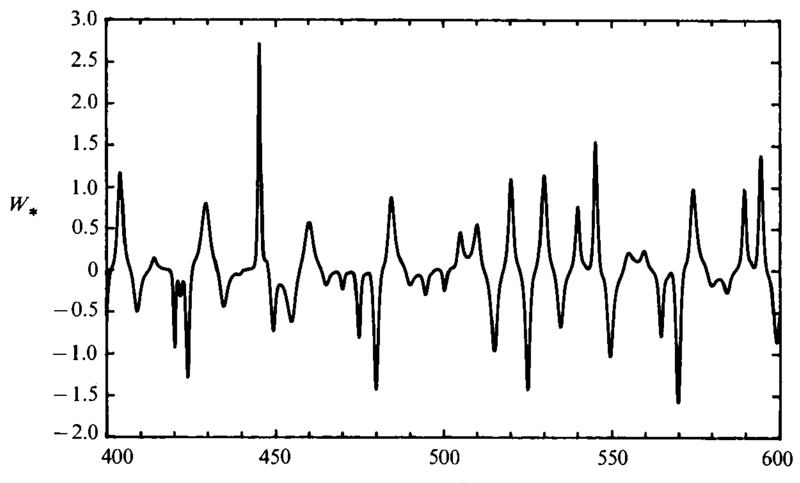

FIGURE 13. Sample drift velocity.

bubble oscillation clearly provide one mechanism for erratic dancing of a bubble in sound. From their general result (Benjamin & Ellis 1990, equation (6.4)) the mean drift velocity, to the leading order, is

$$\overline{W} = \frac{9R}{3+2n}\overline{\epsilon_n \epsilon_{n+1}} \tag{7.5}$$

for two aligned modes, where the overline represents averaging with respect to the period of oscillation and ϵ_n is related to our amplitude a_n by

$$\epsilon_n = a_n \, e^{-i\sigma_n t} + *. \tag{7.6}$$

For large enough n, $\sigma_n - \sigma_{n+1} = O(\epsilon)$ is small so that

$$\overline{W} = \frac{9R}{3+2n}[a_n a^*_{n+1} e^{i(\sigma_n - \sigma_{n+1})t} + *]. \tag{7.7}$$

In terms of our normalization, it can be shown that

$$\overline{W} = \frac{18R}{3+2n} \frac{C_n C_{n+1} + D_n D_{n+1}}{T_0^2 (Q_0^n Q_0^{n+1} Q_n Q_{n+1})^{\frac{1}{2}}}. \tag{7.8}$$

Using the calculated results for the case of figure 11, i.e. for $R = 0.1$ cm, $\tilde{\Omega} = 0.3$ and $n = 0$, the factor $W_* \equiv (C_n C_{n+1} + D_n D_{n+1})$ is shown in figure 13.

8. Concluding remarks

Based on an asymptotic approximation that permits interacting modes to attain comparable amplitudes, we have deduced the evolution equation for the resonant interaction of the breathing mode with one or several distortion modes. Since the frequency mismatch can be of $O(\epsilon)$, resonance occurs more easily, while the growth is faster, than the mechanism studied by Hall & Seminara (1980). We have shown numerically that for one distortion mode, only with imperfect phase matching can resonance lead to chaos. For two distortion modes, chaos occurs only in the range of $\tilde{\Omega}$ where both modes are unstable when interacting alone with the breathing mode. The routes to chaos are found to be different depending on whether one or two distortion modes are present. Specifically, with one distortion mode, chaos follows a sequence of period-doubling bifurcations, while with two it is after a quasi-periodic 2-torus.

Since for a large enough bubble the spectrum of distortion modes is dense, several distortion modes can be disturbed initially and resonate directly with the breathing mode and indirectly with one another. As the development of chaos may depend strongly on the number of modes, further investigations of many-mode interactions would be very worthwhile. As in the analogous cases of standing gravity or capillary–gravity waves in a basin, parametric resonance of two nearly degenerate modes can arise through cubic coupling. This could occur for two very high distortion modes so that the detuning is very small: $\sigma_n - \sigma_{n+1} = O(\epsilon^2 \omega)$; and extension of the theory of Hall & Seminara (1980) would be needed. Because of the high degree of multiplicity at high n, implied by (3.12*b*), consideration of many modes would be even more important there. Finally a large bubble rises fast in a gravitational environment and may no longer be spherical; these physical complications deserve further studies.

This research is partially supported by the Office of Naval Research (Fluid Mechanics Program Contract N0NR N00014-90-J-1163) and National Science Foundation (Fluid Mechanics and Ocean Engineering Program Grants 8813121-MSM). X. Zhou also acknowledges the support by the Institute of Mechanics, Academia Sinica, Beijing, China for making possible his visit to MIT. All computations were carried out with the Dynamical Systems Software. For explaining its use, Professor Schaffer and Mr Charles Tidd of the University of Arizona have our thanks. Dr K. F. Liu kindly helped with some of the computations.

REFERENCES

Armstrong, J. A., Bloembergen, N., Ducing, J. & Pershan, P. S. 1962 Interactions between light waves in a nonlinear dielectric. *Phys. Rev.* **127**, 1918–1939.

Benjamin, T. B. & Ellis, A. T. 1990 Self-propulsion of asymmetrically vibrating bubbles. *J. Fluid Mech.* **212**, 65–80.

BENJAMIN, T. B. & STRASBERG, M. 1958 Excitation of oscillations in the shape of pulsating bubbles – theoretical work. *J. Acoust. Soc. Am.* **30**, 697(A).

BERGE, P., POMEAU, Y. & VIDAL, C. 1984 *Orders within Chaos.* Wiley.

CARR, J. 1981 *Applications of Center Manifold Theory.* Springer.

CILIBERTO, S. & GOLLUB, J. P. 1985 Chaotic mode competition in parametrically forced surface waves. *J. Fluid Mech.* **158**, 381–398.

ELLER, A. J. 1970 Damping constants of pulsating bubbles. *J. Acoust. Soc. Am.* **47**, 1469–1470.

ELLER, A. J. & CRUM, L. A. 1970 Instability of the motion of a pulsating bubble in a sound field. *J. Acoust. Soc. Am.* **47**, 762–766.

FENG, Z. C. & SETHNA, P. R. 1989 Symmetry-breaking bifurcations in resonant surface waves. *J. Fluid Mech.* **199**, 495–518.

GOLLUB, J. P. & MEYER, C. W. 1983 Symmetry-breaking instabilities on a fluid surface. *Physica* D**6**, 337–346.

GU, X. M. & SETHNA, P. R. 1987 Resonant surface waves and chaotic phenomena. *J. Fluid Mech.* **183**, 543–565.

HALL, P. & SEMINARA, G. 1980 Nonlinear oscillations of non-spherical cavitation bubbles in acoustic fields. *J. Fluid Mech.* **101**, 423–444.

HATWAL, H., MALLIK, A. K. & GHOSH, A. 1983 Forced nonlinear oscillations of an autoparametric system – Part 2: Chaotic responses. *Trans. ASME* E: *Appl. Mech.* **50**, 663–668.

KAMBE, T. & UMEKI, M. 1990 Nonlinear dynamics of two-mode interactions in parametric excitation of surface waves. *J. Fluid Mech.* **212**, 373–393.

KAPLAN, J. & YORKE, J. 1979 Chaotic behavior of multidimensional difference equations. In *Functional Differential Equations and the Approximation of Fixed Points* (ed. H. O. Peitgen & H. O. Walther). Springer.

LAMB, H. 1932 *Hydrodynamics*, 6th edn. Cambridge University Press (Dover edition 1945).

LAUTERBORN, W. & PARLITZ, U. 1988 Methods of chaos physics and their application to acoustics. *J. Acoust. Soc. Am.* **84**, 1975–1983.

LONGUET-HIGGINS, M. S. 1989*a* Monopole emission of sound by asymmetric bubble oscillations. Part 1. Normal modes. *J. Fluid Mech.* **201**, 525–541.

LONGUET-HIGGINS, M. S. 1989*b* Monopole emission of sound by asymmetric bubble oscillations. Part 1. An initial-value problem. *J. Fluid Mech.* **201**, 543–565.

LORENZ, E. N. 1963 Deterministic nonperiodic flow. *J. Atmos. Sci.* **20**, 130–141.

MEI, C. C. 1989 *Applied Dynamics of Ocean Surfaces Waves.* World Scientific.

MEI, C. C. & ÜNLÜATA, U. 1972 Harmonic generation in shallow water waves. In *Waves on Beaches* (ed. R. E. Meyer), pp. 181–202. Academic.

MERON, E. & PROCACCIA, I. 1986 Low dimensional chaos in surface waves. Theoretical analysis of an experiment. *Phys. Rev.* A **34**, 3221–3237.

MILES, J. 1984 Resonantly forced motion of two quadratically coupled oscillators. *Physica* **13D**, 247–260.

MINNAERT, M. 1933 On musical air bubbles and the sound of running water. *Phil. Mag.* **16**, 235.

PROSPERETTI, A. 1977 Thermal effects and damping mechanisms in the forced radial oscillations of gas bubbles in liquids. *J. Acoust. Soc. Am.* **61**, 17–27.

RAND, R. H. & ARMBRUSTER, D. 1987 *Perturbation Methods, Bifurcation Theory and Computer Algebra.* Springer.

SETHNA, P. R. 1965 Vibrations of dynamical systems with quadratic nonlinearities. *Trans. ASME* E: *J. Appl. Mech.*, Sept., pp. 576–582.

SIMONELLI, F. & GOLLUB, J. P. 1989 Surface wave mode interaction: effects of symmetry and degeneracy. *J. Fluid Mech.* **199**, 471–494.

STRASBERG, M. & BENJAMIN, T. B. 1958 Excitation of oscillations in the shape of pulsating bubbles experimental work. *J. Acoust. Soc. Am.* **30**, 697(A).

WIJNGAARDEN, L. VAN 1972 One dimensional flow of liquids containing small gas bubbles. *Ann. Rev. Fluid Mech.* **4**, 369–396.

WIJNGAARDEN, L. VAN 1980 Sound and shock waves in bubbly liquids. In *Cavitation and Inhomogeneities in Underwater Acoustics* (ed. W. Lauterborn), pp. 127–140. Springer.